Modulation of Band Bending of Gallium Arsenide with Oriented Helical Peptide Monolayers

Thomas Kaindl,[†] Klaus Adlkofer,[‡,§] Tomoyuki Morita,[§] Junzo Umemura,[#] Oleg Konovalov,[¶] Shunsaku Kimura,*[,§] and Motomu Tanaka*[,†,‡,+]

Physical Chemistry of Biosystems, Institute of Physical Chemistry, University of Heidelberg, D69120 Heidelberg, Germany, Biophysics Laboratory E22, Technische Universität München, D85748 Garching, Germany, Department of Material Chemistry, Graduate School of Engineering, Kyoto University, 615-8510 Kyoto, Japan, Institute of Chemical Research, Kyoto University, 611-0011 Kyoto, Japan, European Synchrotron Radiation Facility, 6 rue Jules Horowitz, 38000 Grenoble, France, Cell Biophysics Laboratory, Institute of Toxicology and Genetics, Karlsruhe Institute of Technology, D76021 Karlsruhe, Germany

Received: October 22, 2010; Revised Manuscript Received: October 29, 2010

We propose a strategy to modulate the electronic structure of gallium arsenide (GaAs) semiconductors by the covalent deposition of uniform monolayers of helical peptides. After the optimization of coupling groups and reaction conditions, structures of peptide monolayers on GaAs were characterized by the combination of grazing incidence-X-ray scattering and Fourier transform infrared spectroscopy yielding the thickness, the area occupied by one peptide helix, and the tilt angle of helical axis with respect to the surface normal. The deposition of the same peptides on high electron mobility transistor (HEMT) devices resulted in a clear change in the carrier mobility depending on the length of peptide helices. The obtained results demonstrated that the macrodipole potential of oriented peptide helices can be utilized for flexible tuning of the electronic structure (band bending) of semiconductors, which can offer a unique alternative to the commonly used doping of charge carriers.

Introduction

Physical properties of semiconductors are dictated by their crystalline structures, and thus changing the composition (e.g., via doping) is the conventional way to change the properties within narrow limits. Chemical functionalization of semiconductor surfaces with organic molecules draws attention as a new strategy to more flexibly modulate the electronic structures of solid-based devices. For example, the deposition of organic molecules onto semiconductor surfaces would lead to a change in surface charges (monopoles) and dipoles, which results in a change in electron affinity and band bending.[1,2] Modifications toward functional moieties at the interface enable chemical sensing in air as well as in water. Functionalization with biomacromolecules, such as DNA[3] and enzymes,[4,5] can readily introduce a variety of biochemical functions toward the fabrication of sensors with high selectivity and sensitivity.

Among various semiconductor materials, gallium arsenide (GaAs) based hybrid materials are promising candidates for fabrication of nanoscale, low-dimensional systems because of their flexibility in band gap engineering.[6,7] Especially, high electron mobility transistors (HEMT) based on undoped GaAs and *n*-AlGaAs heterostructures realize high charge carrier mobility owing to little impurity-induced scattering and are thus promising for high speed switching devices with low electrical noises.[8] There have been several reports on bulk GaAs that chemically functionalize the surface with inorganic and organic mercapto compounds,[9−12] quantum dots,[13] and two-dimensional electron gas devices[14] in vacuum or in air. More recently, we have demonstrated that the enrichment of elemental arsenide by photochemical etching[15,16] or the use of biphenylthiol monolayers[17−19] can overcome the irreversible electrochemical degradation (corrosion) of GaAs under physiological conditions. In the following accounts, we have demonstrated that such functionalized GaAs and two-dimensional electron gas devices can be operated in aqueous buffer to detect the solvent polarity[20] and subphase pH.[21] In fact, the deposition of lipid membranes on functionalized GaAs enables us to determine not only the change in surface charge density with an accuracy of one charge per 60 nm^2 but also the enzymatic degradation of lipid membranes as a function of time.[22]

To date, several synthetic molecules that have donor-sensitizer or sensitizer-acceptor dyads[23] as well as donor-sensitizer-acceptor triads[24] have been deposited on Au showing their capability of efficient photocurrent generation. Instead of small organic molecules with hydrocarbon chain linkers, Miura et al. further extended the strategy and made use of helical peptides as the building blocks. Helical peptides can be considered as rigid rods with diameters of approximately 1−1.5 nm that possess little conformational degrees of freedom under various conditions. Actually, helical peptides with disulfide coupling groups can form monolayers on Au(111) substrates showing tilt angles of 30° to the direction normal to the surface.[25] The unique advantage of helical peptides over commonly used small thiol derivatives is the fact that they possess much larger macrodipole moments along the helical axis proportional to the number of bonds.[26] For example, the H−, CH_3−, and HO− terminal groups of organic thiols (e.g., alkanethiols and biphenyl thiols) possess dipole moments below 1.3 D,[27] while that of a

* To whom correspondence should be addressed. E-mail: shun@scl.kyoto-u.ac.jp (S. K.); tanaka@uni-heidelberg.de (M. T.).
[†] University of Heidelberg.
[‡] Technische Universität München.
[§] Graduate School of Engineering, Kyoto University.
[#] Institute of Chemical Research, Kyoto University.
[¶] European Synchrotron Radiation Facility.
[+] Karlsruhe Institute of Technology.

10.1021/jp110133t © XXXX American Chemical Society

CHART 1: Chemical Structures of Peptides Used in This Study[a]

LipoL16B

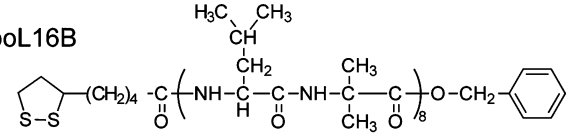

AcSL16B

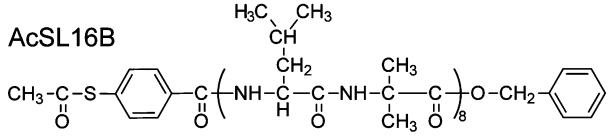

AcSL8B

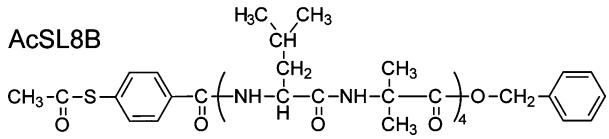

[a] AcSL8B and AcSL16B with thioacetylphenyl groups were treated with NH_4OH to deprotect the thiol groups.

helical peptide with 16 amino acids can amount to 50 D.[26,27] In fact, we successfully demonstrated that helical peptides with photosensitizers grafted on Au surfaces can be used as a molecular photodiode, which can regulate the photocurrent by the direction of the dipole moments[28] and the wavelength of the excitation.[29]

In the present paper, we established the functionalization of GaAs(100) with monolayers of helical peptides of different lengths that possess thiol coupling groups at one end. The formation of uniform peptide monolayers on GaAs can be confirmed by ellipsometry and atomic force microscopy (AFM). The thickness, roughness, and electron density profiles perpendicular to the substrate are measured by grazing incidence X-ray scattering out of specular plane (GIXOS) that can offer a unique advantage to minimize the radiation damage to organic compounds. Furthermore, the orientation of peptide helices can quantitatively be calculated from the ratio between amide I and amide II bands obtained from transmission absorption Fourier transform infrared (TM-FTIR) spectroscopy. The influence of macrodipole moments on the electronic structure (band bending) of GaAs can be observed by the Kelvin probe measurements of bulk, p-doped GaAs substrates and current−voltage ($I-V$) characteristics of HEMT devices. Although quantitative evaluations of the contact potentials and $I-V$ characteristics are still difficult, the observed tendency shows an excellent agreement from the density and orientation of peptide helices calculated from the GIXOS and TM-FTIR results.

Experimental Section

Materials. Undoped, single-side polished GaAs(100) wafers of thickness 355 μm from Wafer Technology Ltd. (Bucks, United Kingdom) were used for all the structural characterizations (AFM, ellipsometry, and GIXOS), while undoped, double-sided polished GaAs(100) wafers from Freiberger GmbH (Freiberg, Germany) were for TM-FTIR experiments. The wafers were cleaved into 1×1 cm^2 pieces for AFM and into 2×2 cm^2 pieces for ellipsometry, TM-FTIR, and GIXOS experiments. GaAs HEMTs that consist of two gold contact pads for source, gate, and drain in a nonencapsulated design are generous gifts from Eudyna Devices Inc. (Yokohama, Japan). The chemical structure of all peptides used in this study (LipoL16B, AcSL16B, and AcSL8B) are shown in Chart 1, whose syntheses were reported previously.[25,30] All peptides form stable α-helical[31] parts with repeat units of leucine (Leu) and aminoisobutyric acid (Aib). LipoL16B has a disulfide coupling group, while the other two (AcSL16B and AcSL8B) have thioacetylphenyl groups at the N-terminal. All the other chemicals were purchased from Sigma Aldrich (Steinheim, Germany) and were used without further purification. Throughout this study, double-deionized water with a specific resistance $R > 18$ MΩcm (Millipore, Molsheim, France) was used.

Sample Preparation. Prior to the surface modification, the substrates were sonicated in acetone for 30 s and were rinsed with ethanol. The native oxide layer of GaAs was removed by immersing the sample in 37% HCl for 1 min resulting in a stoichiometric GaAs(100) surface.[32] To remove the remaining HCl without reoxidation, the sample was briefly rinsed with H_2O and was transferred immediately into the glass reactor with 5 mL portions of 100 μM peptide solution in ethanol. The reaction was carried out under nitrogen (N_2) atmosphere in order to avoid surface oxidation. Prior to the coupling reaction, AcSL8B and AcSL16B with thioacetylphenyl groups were treated with 7 μL NH_4OH (30%) to deprotect the thiol groups. After the monolayer deposition, the samples were thoroughly rinsed with ethanol, were dried by N_2 jet, and were stored in N_2 atmosphere.

Ellipsometry. Experiments were carried out with a point ellipsometer (Optrel, Berlin, Germany) at a constant wavelength of $\lambda = 632.8$ nm and at a fixed angle of incidence of 70°. The refractive index of a GaAs substrate was determined to be $n - ik = 3.81 - i0.31$ showing good agreement with the literature.[33] By assuming the refractive index[34] for peptides to be $n = 1.5$, the thickness of the monolayer was calculated out of five independent measurements.

Atomic Force Microscopy (AFM). All measurements were performed in tapping mode with a Nanoscope IIIa AFM (Digital Instruments, Mannheim, Germany) using silicon cantilevers with a spring constant of ∼42 N/m and a tip radius of <10 nm (NanoAndMore GmbH, Wetzlar, Germany). The scanning speed was kept below 1 Hz for scan areas between 1×1 μm^2 and 5×5 μm^2. Typical modulation in amplitude and frequency were about 10 nm and 300 kHz, respectively. The images were subjected to a plane correction procedure.

Grazing Incidence X-ray Scattering Out of Specular Plane (GIXOS). GIXOS measurements were conducted at ID10B beamline of the European Synchrotron Radiation Facility (ESRF, Grenoble). A monochromatic incident beam ($E = 8.01$ keV, $\lambda = 1.55$ Å) was collimated with slits of 300 mm × 100 mm in horizontal and vertical orientations, respectively. The sample was illuminated at an incident angle of $\alpha_i = 0.24°$ corresponding to approximately 80% of the angle of total reflection for the GaAs/air interface, $\alpha_c = 0.31°$. Here, the penetration depth of the evanescent wave $\Lambda = 36$ Å can be calculated from the angle of incidence α_i[35]

$$\Lambda \cong \frac{1}{q_c}\sqrt{\frac{\alpha_c^2}{\alpha_c^2 - \alpha_i^2}} \qquad (1)$$

where q_c is the momentum transfer at the critical angle α_c, $q_c = (4\pi/\lambda)\sin\alpha_c$. The sample was kept in He atmosphere to avoid scattering in air as well as to minimize the radiation damage. We inserted a Soller collimator before a linear position-sensitive detector (PSD) to achieve the angular resolution of 0.03°. The intensity of the scattered beam is collected with a PSD standing perpendicular to the sample surface at a fixed small azimuth angle $\delta = 0.34°$ corresponding to the in-plane momentum

transfer of $q_{||} \sim 0.029$ Å^{-1}. Provided that the in-plane momentum transfer is very small ($q_{xy} \sim 0$) and that the interface roughness is conformal, the measured diffuse intensity can be connected to the corresponding reflectivity curve[36]

$$I(q_z) \propto |T(k_{in})|^2 |T(k_{out})|^2 \frac{R(q_z)}{R_F(q_z)} \quad (2)$$

$I(q_z)$ denotes the intensity measured in a GIXOS experiment, $R(q_z)$ is the corresponding specular reflectivity as measured in a $\theta-2\theta$ scan, $R_F(q_z)$ denotes the Fresnel reflectivity from a flat (ideal) surface, and $T(k_{in})$ and $T(k_{out})$ represent the characteristic Vineyard Function for the grazing incidence configuration. The diffuse scattering can be described within the kinematical approach using the Master-Formula[35]

$$R(q_z) = R_F(q_z)\left|\frac{1}{\rho}\int \frac{d\rho(z)}{dz}\exp(iq_z z)dz\right|^2 \quad (3)$$

The electron density of bulk GaAs, $\rho_{GaAs} = 38.5 \times 10^6$ e$^-$/Å^2, was calculated and was used as a fixed constant. The experimental data were fitted using a self-written routine based on a slab model in order to achieve the least-squares fit for the electron density ρ and thickness d of the peptide layer as well as the roughness values for the peptide/air (σ_1) and the peptide/GaAs interface (σ_2). The data points below $q_z = 0.06$ Å^{-1} are not included in the fit since the Master-Formula is no longer valid at $q_z < 2 \times q_c$.[35]

Transmission Fourier Transformed Infrared Spectroscopy (TM-FTIR). FTIR spectra were measured using a Bruker IFS 66/s FTIR spectrometer (Ettlingen, Germany) in transmission mode at wave numbers ν between 4000 cm^{-1} and 600 cm^{-1} with a resolution of 4 cm^{-1}. The measurement curve was accumulated from 2000 interferogram repetitions at a fixed incident angle θ of 40°. To exclude the influence of the instrumental IR intensity distribution and the absorption spectrum of the substrate, the background signal was subtracted from the untreated GaAs spectrum.

Current−Voltage ($I-V$) Characteristics of HEMTs. Prior to the surface modification of HEMT chips, we removed the protection layer on the HEMT by wet chemical etching with HF (Si_3N_4, personal communication). Immediately after the wet chemical etching, the sample was quickly rinsed with H_2O and was dried by a N_2 flow. The current−voltage ($I-V$) characteristics of HEMT chips before and after the functionalization were measured with a PSM6 chip tester (Suss MicroTec AG, Garching, Germany) by contacting the chip with tungsten needles with a tip radius of 7 μm (American Probe & Technologies, Milpitas, CA, United States). A voltage V_{SD} was applied from source to drain by the first Keithley K2400 source-meter, while the gate potential was regulated through a voltage drop from source to gate V_{GS} by the second source-meter (Keithley Instruments GmbH, Germering, Germany). Both the source and the sample stage were carefully grounded to avoid any undesired interference from stray capacitance or electric noise. The relationships between the source−drain current I_{SD} versus V_{GS} were monitored at constant $V_{SD} = 0.5$ V, and I_{SD} versus V_{SD} was recorded for fixed V_{GS} between 0 and 1 V using a self-written software in LabView (National Instruments, Austin, TX, United States). $I-V$ characteristics of etched samples mean those in the presence of native oxide since it is practically impossible to build the HEMT into the chip tester before the reoxidation of the surface.[15]

Calculation of Molecular Orientation. The orientation of helical peptide molecules on planar, stratified samples was calculated from the absorption ratio between amide I and amide II bands in the FTIR spectra. In contrast to previous accounts,[25,30] we assumed a slab model that consists of air (layer 0), peptide (layers 1 and 3), and GaAs (layer 2) layers, which is consistent with interpretation of our GIXOS results. The transmission through stratified layers with different refractive indices was calculated by the Abelès matrix formalism[37] for an electric field vector E traveling forward and backward using a 2×2 scattering matrix S.[38] Since the monolayers of helical peptides possess birefringence, both parallel (p) and perpendicular (s) components of the electric field vector E are altered. The amplitudes of reflection and transmission coefficients at anisotropic interfaces (r_{ij} and t_{ij}, respectively) were theoretically derived in previous accounts.[39,40] In the case of uniaxial crystals in basal orientation, they reduced to the Fresnel equations that use the optical functions $\hat{n} + i\kappa$ for each slab material. We used the literature values for GaAs,[34] whereas for peptides, the refractive index $\hat{n}$ was simulated as anomalous dispersion curve[41] from a Lorenzian spectral line shape near each amide absorption peak (ν_I and ν_{II}). The off-resonant mid-IR value was set to $n_{inf} = 1.5$. The extinction coefficients κ_{xy} and κ_z of a helical peptide layer can be calculated for each amide band from Fraser's equations[42]

$$\kappa_{xy} = \kappa_{max}\left(\frac{1}{2}f\sin^2\alpha + \frac{1}{3}(1-f)\right)$$

$$\kappa_z = \kappa_{max}\left(f\cos^2\alpha + \frac{1}{3}(1-f)\right) \quad (4)$$

Here, α is the angle between the maximum transition dipole of each amide band and the director axis of the molecule, $\alpha_I = 39°$ and $\alpha_{II} = 75°$ for an α-helix (16mer peptide) or $\alpha_I = 39°$ and $\alpha_{II} = 83°$ for a 3_{10}-helix (8mer peptide),[43−46] and κ_{max} is the maximum transition strength for each amide band. In this study, we quantitatively calculated these values from the extinction coefficients and molar concentrations of each group with an aid of GIXOS results (see the following section). The order parameter f is a function of the molecular tilt γ with respect to the surface normal averaged over time

$$f = \frac{1}{2}\langle 3\cos^2\gamma - 1\rangle \quad (5)$$

Repeated application of the matrix formalism for each slab interface results in an overall scattering matrix S_n. Its first entry corresponds to the transmittance through n slabs for p- and s-polarized lights

$$T_{n,p} = \frac{1}{S^{11}_{n,p}} \text{ and } T_{n,s} = \frac{1}{S^{11}_{n,s}} \quad (6)$$

The total absorbance A is the average of $A_{n,p} = -\log(T_{n,p}/T_{GaAs,p})$ and $A_{n,s} = -\log(T_{n,s}/T_{GaAs,s})$, where T_{GaAs} represents the transmittance through the bare GaAs substrate

$$A = (A_p + A_s)/2 \quad (7)$$

TABLE 1: Thicknesses of AcSL8B and AcSL16B Monolayers on GaAs[100] Substrates for Grafting Reactions at 50 °C[a]

grafting time	10 h	20 h	40 h	50 h
AcSL8B	5−10 Å	18 Å	18 Å	
AcSL16B	5−10 Å	28 Å	28 Å	28 Å

[a] The molecules that are not covalently anchored to the surface were removed by the sonication in EtOH for 1 min. After 20 h, the final thickness values, $d_{AcSL8B} = 18 \pm 5$ Å and $d_{AcSL16B} = 28 \pm 5$ Å, could be obtained.

Therefore, the tilt angle γ can be calculated from the absorption ratio $A(\nu_I)/A(\nu_{II})$ of two given amide peaks ν_I and ν_{II} since the absorption spectra are determined by wavenumber ν and order parameter f (and thus γ).

Results and Discussion

Optimization of Grafting Conditions. As the first step, conditions for the grafting reactions were optimized. The quality of the peptide layers was evaluated by measuring the film thickness with ellipsometry. The influence of the reaction temperature on the quality of LipoL16B monolayers was checked by grafting reactions at $T = 20$, 50, and 80 °C for 20 h. The reactions at 20 and 80 °C resulted in a film thickness of below 10 Å. Since the reaction at 50 °C led to an increase in the film thickness, we carried out the reaction at 50 °C for 10, 20, 40, 50, and 80 h in order to optimize the reaction time. We observed a monotonic increase in the film thickness according to the reaction time, which reached saturation after 40 h. After 40 h, we observed no remarkable change in the film thickness. However, the subsequent sonication of all the samples for 1 min in EtOH resulted in a remarkable decrease in the layer thickness (<10 Å). This finding suggests the partial desorption of LipoL16B molecules because of a low yield of covalent coupling. Similar noneffective disulfide binding on GaAs was previously reported for 1-octadecyldisulfanyl-octadecane.[47] In contrast, AcSL8B and AcSL16B seemed to establish more stable layers. Although the optimal temperature for the grafting reaction for both molecules was also found to be 50 °C (Table 1), the film thickness of AcSL8B and AcSL16B saturated already after 20 h to $d_{AcSL8B} = 18 \pm 5$ Å and $d_{AcSL16B} = 28 \pm 5$ Å, respectively. The errors (±5 Å) were from five independent ellipsometry measurements. A longer reaction time led to the formation of films with thickness greater than 50 Å, but a short sonication was sufficient to recover the thickness values to $d_{AcSL8B} = 18 \pm 5$ Å and $d_{AcSL16B} = 28 \pm 5$ Å. Thus, we focus on AcSL8B and AcSL16B deposited on GaAs substrates at 50 °C for 20 h in the following sections.

Surface topography of GaAs before and after the functionalization was characterized by tapping mode AFM at several different locations within scan areas of 1×1 μm^2 and 5×5 μm^2. Figure 1 shows AFM topographic images of GaAs(100) substrates coated with (A) AcSL8B and (B) AcSL16B. The deposition of a peptide monolayer resulted in a uniform coverage of the substrates. Within the scan area of 1×1 μm^2, the root-mean-squared (rms) roughness of the AcSL8B monolayer is $\sigma_{AcSL8B} = 5.4$ Å and that of the AcSL16B monolayer is $\sigma_{AcSL16B} = 7.9$ Å. These values are slightly larger than that of a freshly etched GaAs(100) surface, $\sigma_{GaAs} = 3.5$ Å.[18] The obtained results confirm that the wet chemical etching of native oxide as well as the deposition of the peptide monolayer did not cause remarkable changes in the surface roughness. The comparable rms roughness values in the absence and presence of peptide

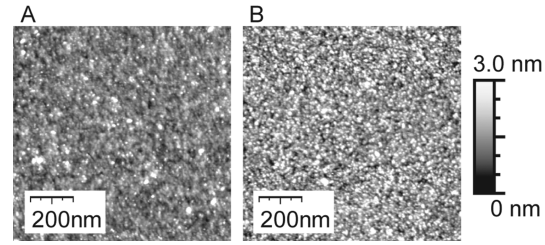

Figure 1. Tapping mode AFM images of GaAs(100) coated with (A) AcSL8B and (B) AcSL16B. The rms roughnesses within 1×1 μm^2 are (A) 5.4 Å and (B) 7.9 Å, respectively.

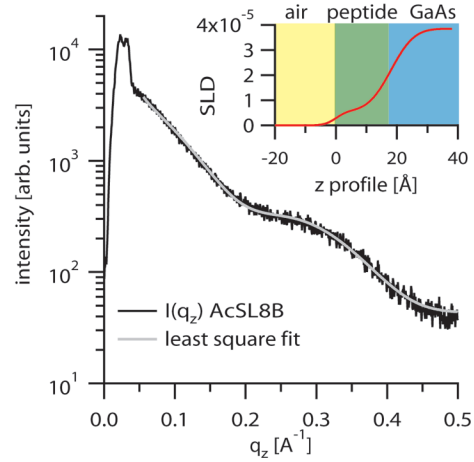

Figure 2. GIXOS signal (black) and the least-squares fit (gray) for the AcSL8B monolayer on GaAs(100). The electron density profile perpendicular to the surface reconstructed from the GIXOS result is presented as an inset. The air/peptide interface was set as $z = 0$.

TABLE 2: Summary of GIXOS Results for Peptide Monolayers on GaAs(100)[a]

GIXOS	SLD [$\times 10^{-6}$ Å^{-2}]	D [Å]	σ_{01} [Å]	σ_{12} [Å]
AcSL8B	5.6	18.0	2.9	6.0
AcSL16B	5.3	31.0	9.2	7.0

[a] SLD, scattering length density; d, monolayer thickness; σ_{01}, roughness of the air/peptide interface; σ_{12}, roughness of the peptide/GaAs interface.

monolayers confirm that the roughness of each interface remains conformal, which is the prerequisite for GIXOS measurements.[36]

The fine structures (thickness, roughness, and electron density profiles) of the peptide monolayers perpendicular to the substrate were further characterized by GIXOS. Figure 2 represents the measured GIXOS signals (black) and the corresponding best fit model based on the one slab model (gray) for the AcSL8B monolayer on GaAs(100). The scattering length density (SLD) profile reconstructed from the best fit result is presented as an inset. The thickness of the AcSL8B layer was calculated to be $d_{AcSL8B} = 18.0$ Å. The roughness of the air/peptide interface σ_{01} and that of peptide/GaAs interface σ_{12} was $\sigma_{01} = 2.9$ Å and $\sigma_{12} = 6.0$ Å, respectively. The corresponding values for the AcSL16B monolayer were calculated to be $d_{AcSL16B} = 31.0$ Å, $\sigma_{01} = 9.2$ Å, and $\sigma_{12} = 7.0$ Å. As summarized in Table 2, the peptide layer thickness values calculated from the GIXOS result showed good agreement with the mean value of the ellipsometric thickness, $d_{AcSL8B} = 18$ Å and $d_{AcSL16B} = 28$ Å, respectively. We regard the thickness values derived from GIXOS as more reliable ones since the pseudo-optical constant of freshly etched GaAs calculated for ellipsometry may be altered by the electronic structure of S−As bonds at the interface.[48] As presented in previous studies,[15,47] here we used ellipsometry for

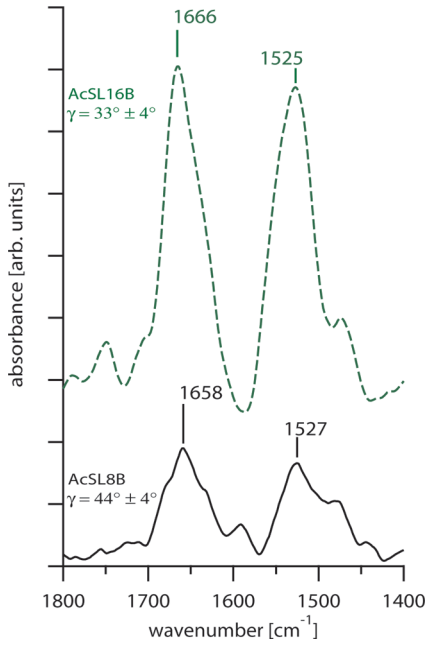

Figure 3. TM-FTIR spectra of AcSL8B (solid line) and AcSL16B (broken line) on GaAs(100) measured at an incidence angle $\theta = 40°$.

a rough estimation of the film thickness to optimize grafting conditions. Also, the rms roughness values of the air/peptide interface obtained by AFM and GIXOS increase according to the elongation of peptide helices, although they are estimated in two different manners: σ_{01} measured by GIXOS coincides with the gradual change in the electron density across the interface and σ_{AcSLXB} measured by AFM is calculated from the topographic height difference. Furthermore, the lateral density of peptide molecules in the monolayer can be gained by the SLD of slab 1 (peptide layer), $SLD_{AcSL8B} = 5.6 \times 10^{-6}$ Å^{-2} and $SLD_{AcSL16B} = 5.3 \times 10^{-6}$ Å^{-2}. Here, the area A occupied by one peptide molecule can be calculated

$$A_{AcSLXB} = \frac{r_e \times N_e}{SLD \times d_{AcSLXB}} \tag{8}$$

where r_e is the Thomson electron radius, N_e is the total number of electrons per molecule, and d_{AcSLXB} is the peptide layer thickness obtained by GIXOS. We calculated the areas occupied by one AcSL8B and AcSL16B molecule from the thickness obtained by GIXOS (Table 2), $A_{AcSL8B} = 135$ Å^2 and $A_{AcSL16B} = 150$ Å^2. The value for AcSL16B seems to agree very well with that of a peptide with the same repeat units (but with no thiol group) measured at the air/water interface, $A \sim 150$ Å^2,[41] suggesting that AcSL16B molecules form a highly packed monolayer on GaAs(100).

Figure 3 shows the TM-FTIR spectra of GaAs(100) coated with the monolayers of AcSL8B (solid line) and AcSL16B (broken line) measured at an incidence angle of $\theta = 40°$. The FTIR spectrum of AcSL8B shows two absorption peaks at $\nu_I = 1658$ cm^{-1} and $\nu_{II} = 1527$ cm^{-1}, which are characteristic for amide I and amide II bands of helical peptides, respectively.[49,50]

To simulate the measured FTIR spectra, the maximum transition strength κ_{max} for each amide band is calculated according to Beer's law

$$\kappa_{maxI} = \frac{2.3 \cdot \varepsilon \cdot \rho}{\nu \cdot 4\pi} \tag{9}$$

Here, the extinction coefficient ε of amide I and amide II bands can be measured by absorption spectra of the same peptides in solutions ($\varepsilon_I = 124$ m^2 mol^{-1} and $\varepsilon_{II} = 76$ m^2 mol^{-1}). The molar concentration of amide groups ρ for AcSL8B ($n = 8$) can be deduced from the volume per molecule measured by GIXOS, $\rho_{AcSL8B} = n/(A_{AcSL8B} \times d_{AcSL8B} \times N_A) = 5466$ mol m^{-3}, where N_A is Avogadro's number. This yields the maximum transition strength $\kappa_{maxI} = 0.74$ and $\kappa_{maxII} = 0.50$ for AcSL8B. Following the same steps, the corresponding values for AcSL16B ($\kappa_{maxI} = 0.78$ and $\kappa_{maxII} = 0.52$) can be calculated from $\rho_{AcSL16B} = 5713$ mol m^{-3}. Since the absorption of each amide band depends on the order parameter f, the tilt angle γ of AcSL8B and AcSL16B with respect to the surface normal can be calculated, $\gamma_{AcSL8B} = 44 \pm 4°$ and $\gamma_{AcSL16B} = 33 \pm 4°$. Molecular space filling modeling with subsequent force field (MM2) minimization for the helical peptides lacking the protecting acetyl group (abbreviated as HSL8B and HSL16B here) yields peptide lengths of 28 Å for HSL8B and 39 Å for HSL16B. In another approach, one can estimate a translation of 1.5 Å per residue for an α-helix or 2.0 Å per residue for a 3_{10}-helix and add 6 Å each for terminating thiophenylcarbonyl and oxybenzyl groups yielding 28 Å for HSL8B and 36 Å for HSL16B, respectively. The molecular lengths calculated by the GIXOS monolayer thicknesses and the FTIR tilt angles (25 Å for the AcSL8B monolayer and 37 Å for the AcSL16B monolayer) seem to be in good agreement with the values predicted from two different approaches.

After the characterization of the monolayers on bulk GaAs(100), the peptide monolayers were deposited onto GaAs HEMTs. After the deposition of peptide monolayers, all HEMT devices were operational at various V_{GS} (Supporting Information) showing no sign of degradation throughout the experiments (~10 h). The removal of the protection layer by wet chemical etching resulted in a significant decrease in the source−drain current I_{SD} for variable source−drain voltages V_{SD} and a fixed $V_{GS} = 0$ V (Supporting Information). The characterization of bare GaAs is not possible since the surface is rapidly oxidized in ambient atmosphere.[15] More significant changes in I_{SD} could be observed in the presence of AcSL8B and AcSL16B monolayers. Figure 4 shows the current−voltage ($I_{SD}-V_{GS}$) curves of an as-received HEMT device (blue), an HEMT after the removal of the protection layer (red), and HEMTs coated with AcSL8B (black) and AcSL16B (green) measured at a fixed source−drain voltage of $V_{SD} = 0.5$ V. The slope of this graph is referred to as transconductance of a transistor g_m[51]

$$g_m = \left[\frac{\partial I_{SD}}{\partial I_{GS}}\right]_{V_{SD}=const} \tag{10}$$

For small gate voltages V_{GS} at fixed $V_{SD} = 0.5$ V, the HEMT operates in a linear regime, where we measured the same transconductance as specified by the manufacturer ($g_m = 50$ mS). After removal of the protection layer, g_m decreases only slightly to 46 mS. HEMTs coated with AcSL8B and AcSL16B showed about 2.7 times reduced transconductance of $g_m = 18$ mS and $g_m = 16$ mS, respectively. The threshold potential V_T can be derived from the extrapolated intersection points between a linear fit of the $I_{SD}-V_{GS}$ at fixed V_{SD} and the V_{GS} axis (dashed lines in Figure 4)[52] yielding a clear difference between AcSL8B and AcSL16B, $\Delta V_T = 82$ mV. Previously, Imanishi et al. measured the contact potential of Au substrates coated with disulfide-functionalized peptides using a Kelvin probe and reported the potential difference between short (8 amino acids)

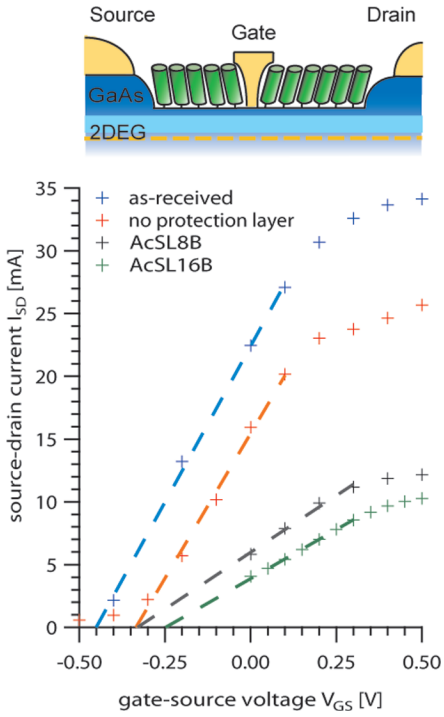

Figure 4. Source−drain current I_{SD} for different gate potentials V_{GS} at a fixed source−drain voltage of $V_{SD} = 0.5$ V in the linear regime. The transconductance g_m is gained as slope from a linear fit.

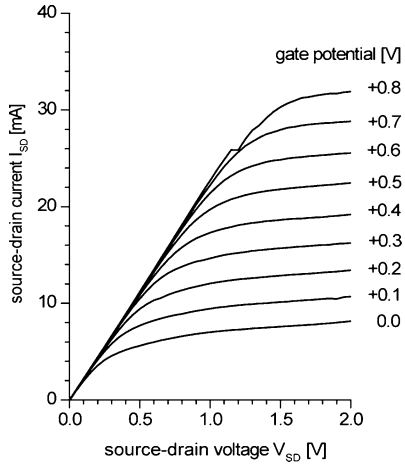

Figure 5. $I_{SD}-V_{SD}$ characteristics of GaAs HEMT after deposition of AcSL8B on the gate area. The gate voltage step is $V_{GS} = 0.1$ V.

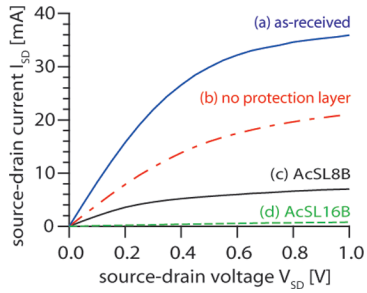

Figure 6. $I_{SD}-V_{SD}$ curves of (a) as-received HEMT, (b) HEMT with no protection layer, (c) HEMT with AcSL8B, and (d) HEMT with AcSL16B. All the measurements were performed at $V_{GS} = 0$ V.

and long (16 amino acids) helices of $\Delta V \sim 90$ mV.[53] Despite differences in detailed molecular structures, the value we obtained from HEMT experiments seems to agree well with that reported by Imanishi et al. The current device geometry does not allow quantitative determination of the device-specific constants (e.g., carrier mobility and width and length of the conducting channel), however, the results obtained here clearly indicated the capability of peptide molecules to modulate the band bending and thus carrier mobility in the conducting channels in transistor devices.

Owing to the quantitative characterizations of the peptide monolayers presented above, the potentials ΔV_{dip} generated by a dipole moment p can be calculated using the Helmholtz equation

$$\Delta V_{dip} = \frac{p}{\varepsilon \varepsilon_0 A} \cos \gamma \qquad (11)$$

where ε_0 is the electric constant of vacuum. The dielectric constant of nonhydrated peptides ($\varepsilon = 3.5$) was taken from the literature,[54] γ is the angle between the helix axis and the surface normal, and A is the area per dipole moment. As mentioned above, both γ and A can be calculated from FTIR and GIXOS results. In vacuum, the effective molecular dipole moment of helical peptides with eight amino acids (but with no end functionalities) would amount almost up to $p \sim 25$ D.[27] If one takes this value as a crude approximation, the Helmholtz equation yields the dipole potential of $\Delta V_{dip} \sim 1.4$ V. This value is about an order of magnitude larger than the contact potential difference measured on the HEMT device ($\Delta V \sim 82$ mV) and values on Au.[53] This apparent discrepancy may be attributed to several possible reasons. For example, the estimation of the macrodipole moment from the simple sum of all the hydrogen bonds might be erroneous, since dipole−dipole interactions can only reach a short distance and are mainly localized within the first and the last helical turns.[27,55] In addition, the π-electron system of the benzyl ester group located at the C-terminal as well as the covalent As−S bond[18] might cause screening, too.[55] Last but not least, the presence of water in or on the peptide layer cannot be excluded as the experiments were carried out in ambient atmosphere. Even a trace of water ($\varepsilon_{H2O} = 80$) molecules would cause a significant increase in the dielectric constant of peptides from $\varepsilon = 3.5$. For the full calculation of dielectric constants and dipole moments of peptides on GaAs, the combination of detailed theoretical models and experiments in vacuum would be necessary. Last but not least, further chemical modification of peptides with specific recognition groups or functional dyads/triads seems to be a promising strategy toward the optimization of the sensitivity of peptide-functionalized GaAs devices against external stimuli.

Conclusions

We have established the functionalization of GaAs(100) surfaces with helical peptides (8 and 16 amino acids) whose N-termini are functionalized with disulfide or thiol coupling groups. Ellipsometry demonstrated that helical peptides with thiol coupling groups form more stable and uniform layers than the disulfide-functionalized ones. AFM and grazing-incidence X-ray scattering (GIXOS) results confirmed the formation of uniform peptide monolayers on GaAs. The comparison between experimental results and theoretical modeling of FTIR spectra yields the tilt angles of peptide helices with respect to the surface normal. Taking the thickness and electron density obtained from GIXOS, one can quantitatively estimate the impact of dipole potentials from peptide molecules on the electronic structure (band bending) of GaAs. We further transferred the same functionalization protocols on transistor (HEMT) devices. We

observed a significant influence of peptide molecules on the $I-V$ characteristics and conductance (carrier mobility) of HEMT devices, where the changes in the contact potential reflect the length and direction of peptide helices. Because the lateral density of dipoles and the angle between the dipole moments and the surface normal can be deduced from the experimental results, the dipole potentials applied to GaAs can be estimated. Although several parameters, such as dielectric constants and dipoles of peptides on GaAs, should be further refined, the obtained results demonstrate a large potential of this strategy toward the modulation of semiconductor electronic structures using helical peptide molecules.

Acknowledgment. We thank ESRF for the synchrotron beam time and Y. Aoki (Eudyna Inc.) for the practical suggestions. K. A., T. K., and M. T. thank M. Himmelhaus for the helpful comments on the initial FTIR experiments. This work has been supported by the German Science Foundation (SFB 563), the Federal Ministry of Education and Research (13N9109), and the Fonds der Chemischen Industrie. K. A. thanks the DAAD for the postdoctoral fellowship and T. K. is thankful to the State Baden-Württemberg for the doctoral fellowship. M. T. is a member of German Excellence Cluster "CellNetwork", Center for Quantitative Biology (BIOQUANT), and Helmholtz Program "BioInterface".

Supporting Information Available: This material is available free of charge via the Internet at http://pubs.acs.org.

References and Notes

(1) Ashkenasy, G.; Cahen, D.; Cohen, R.; Shanzer, A.; Vilan, A. *Acc. Chem. Res.* **2002**, *35*, 121.
(2) Bergveld, P. *Sens. Actuators, B* **2003**, *88*, 1.
(3) Xu, Y.; Cheng, G. F.; He, P. G.; Fang, Y. Z. *Electroanalysis* **2009**, *21*, 1251.
(4) Arya, S. K.; Solanki, P. R.; Datta, M.; Malhotra, B. D. *Biosens. Bioelectron.* **2009**, *24*, 2810.
(5) Turner, A. P. F. *Science* **2000**, *290*, 1315.
(6) Spirkoska, D.; Abstreiter, G.; Morral, A. F. I. *Semicond. Sci. Technol.* **2009**, 24.
(7) Stutzmann, M.; Garrido, J. A.; Eickhoff, M.; Brandt, M. S. *Phys. Status Solidi A* **2006**, *203*, 3424.
(8) Mimura, T. *Jpn. J. Appl. Phys.* **2005**, *44*, 8263.
(9) Lunt, S. R.; Ryba, G. N.; Santangelo, P. G.; Lewis, N. S. *J. Appl. Phys.* **1991**, *70*, 7449.
(10) McGuiness, C. L.; Blasini, D.; Masejewski, J. P.; Uppili, S.; Cabarcos, O. M.; Smilgies, D.; Allara, D. L. *ACS Nano* **2007**, *1*, 30.
(11) Seker, F.; Meeker, K.; Kuech, T. F.; Ellis, A. B. *Chem. Rev.* **2000**, *100*, 2505.
(12) Sheen, C. W.; Shi, J. X.; Martensson, J.; Parikh, A. N.; Allara, D. L. *J. Am. Chem. Soc.* **1992**, *114*, 1514.
(13) Adlkofer, K.; Duijs, E. F.; Findeis, F.; Bichler, M.; Zrenner, A.; Sackmann, E.; Abstreiter, G.; Tanaka, M. *Phys. Chem. Chem. Phys.* **2002**, *4*, 785.
(14) Vilan, A.; Cahen, D. *Trends Biotechnol.* **2002**, *20*, 22.
(15) Adlkofer, K.; Tanaka, M. *Langmuir* **2001**, *17*, 4267.
(16) Adlkofer, K.; Tanaka, M.; Hillebrandt, H.; Wiegand, G.; Sackmann, E.; Bolom, T.; Deutschmann, R.; Abstreiter, G. *Appl. Phys. Lett.* **2000**, *76*, 3313.
(17) Adlkofer, K.; Eck, W.; Grunze, M.; Tanaka, M. *J. Phys. Chem. B* **2003**, *107*, 587.
(18) Adlkofer, K.; Shaporenko, A.; Zharnikov, M.; Grunze, M.; Ulman, A.; Tanaka, M. *J. Phys. Chem. B* **2003**, *107*, 11737.
(19) Shaporenko, A.; Adlkofer, K.; Johansson, L. S. O.; Tanaka, M.; Zharnikov, M. *Langmuir* **2003**, *19*, 4992.
(20) Luber, S. M.; Adlkofer, K.; Rant, U.; Ulman, A.; Golzhauser, A.; Grunze, M.; Schuh, D.; Tanaka, A.; Tornow, M.; Abstreiter, G. *Physica E* **2004**, *21*, 1111.
(21) Gassull, D.; Luber, S. M.; Ulman, A.; Grunze, M.; Tornow, M.; Abstreiter, G.; Tanaka, M. *J. Phys. Chem. C* **2007**, *111*, 12414.
(22) Gassull, D.; Ulman, A.; Grunze, M.; Tanaka, M. *J. Phys. Chem. B* **2008**, *112*, 5736.
(23) Uosaki, K.; Kondo, T.; Zhang, X. Q.; Yanagida, M. *J. Am. Chem. Soc.* **1997**, *119*, 8367.
(24) Imahori, H.; Yamada, H.; Nishimura, Y.; Yamazaki, I.; Sakata, Y. *J. Phys. Chem. B* **2000**, *104*, 2099.
(25) Miura, Y.; Kimura, S.; Umemura, J. *Langmuir* **1998**, *14*, 6935.
(26) Hol, W. G. J.; Vanduijnen, P. T.; Berendsen, H. J. C. *Nature* **1978**, *273*, 443.
(27) Sengupta, D.; Behera, R. N.; Smith, J. C.; Ullmann, G. M. *Structure* **2005**, *13*, 849.
(28) Morita, T.; Kimura, S.; Kobayashi, S.; Imanishi, Y. *J. Am. Chem. Soc.* **2000**, *122*, 2850.
(29) Yasutomi, S.; Morita, T.; Imanishi, Y.; Kimura, S. *Science* **2004**, *304*, 1944.
(30) Kitagawa, K.; Morita, T.; Kimura, S. *J. Phys. Chem. B* **2004**, *108*, 15090.
(31) Otoda, K.; Kitagawa, Y.; Kimura, S.; Imanishi, Y. *Biopolymers* **1993**, *33*, 1337.
(32) Allongue, P.; Cachet, H. *Ber. Bunsen−Ges. Phys. Chem. Chem. Phys.* **1987**, *91*, 386.
(33) *Landolt-Börnstein: Numerical Data and Functional Relationships in Science and Technologie, Group III: Crystal and Solid State Physics*; Hellwege, K.-H., Ed.; Springer-Verlag: Berlin, 1983; Vol. 17e.
(34) *Handbook of optical constants of solids*; Palik, E. D., Ed.; Academy Press: Orlando, FL, 1985; Vol. 1.
(35) Als-Nielsen, J.; McMorrow, D. *Elements of modern x-ray physics*; Wiley: Chichester, U.K., 2001.
(36) Mora, S.; Daillant, J.; Luzet, D.; Struth, B. *Europhys. Lett.* **2004**, *66*, 694.
(37) Abelès, F. *J. Phys. Radium* **1950**, *11*, 307.
(38) Azzam, R. M. A.; Bashara, N. M. *Ellipsometry and polarized light*; Elsevier: Amsterdam, 2003.
(39) Lekner, J. *J. Phys.: Condens. Matter* **1991**, *3*, 6121.
(40) Thomson, E. S.; Wilen, L. A.; Wettlaufer, J. S. *J. Phys.: Condens. Matter* **2009**, 21.
(41) Kitagawa, K.; Morita, T.; Umemura, J.; Kimura, S. *Polymer* **2002**, *43*, 3533.
(42) Mendelsohn, R.; Brauner, J. W.; Gericke, A. *Annu. Rev. Phys. Chem.* **1995**, *46*, 305.
(43) Tsuboi, M. *J. Polym. Sci.* **1962**, *59*, 139.
(44) Nevskaya, N. A.; Chirgadze, Y. N. *Biopolymers* **1976**, *15*, 637.
(45) Takenaka, T.; Harada, K.; Matsumoto, M. *J. Colloid Interface Sci.* **1980**, *73*, 569.
(46) Yoshida, K.; Kawamura, S.; Morita, T.; Kimura, S. *J. Am. Chem. Soc.* **2006**, *128*, 8034.
(47) McGuiness, C. L.; Shaporenko, A.; Mars, C. K.; Uppili, S.; Zharnikov, M.; Allara, D. L. *J. Am. Chem. Soc.* **2006**, *128*, 5231.
(48) Shi, J.; Hong, B.; Parikh, A. N.; Collins, R. W.; Allara, D. L. *Chem. Phys. Lett.* **1995**, *246*, 90.
(49) Kennedy, D. F.; Crisma, M.; Toniolo, C.; Chapman, D. *Biochemistry* **1991**, *30*, 6541.
(50) Maekawa, H.; De Poli, M.; Toniolo, C.; Ge, N. H. *J. Am. Chem. Soc.* **2009**, *131*, 2042.
(51) Snowden, C. M. *Introduction to semiconductor device modelling*; World Scientific Pub. Co. Inc.: Singapore, 1987.
(52) Sze, S. M. *Semiconductor Devices: Physics and Technologie*; John Wiley & Sons: New York, 1985.
(53) Imanishi, Y.; Miura, Y.; Iwamoto, M.; Kimura, S.; Umemura, J. *Proc. Jpn. Acad., B Phys.* **1999**, *75*, 287.
(54) Brandrup, J.; Immergut, E. *Polymer Handbook*, 3rd ed.; Wiley & Sons Inc., 1989.
(55) Aqvist, J.; Luecke, H.; Quiocho, F. A.; Warshel, A. *Proc. Natl. Acad. Sci. U.S.A.* **1991**, *88*, 2026.

JP110133T